# Ferroelectric Domain Walls in $BaTiO_3$: Fingerprints in XRPD Diagrams and Quantitative HRTEM Image Analysis

N. Floquet ([1,2,*]), C.M. Valot ([2]), M.T. Mesnier ([2]), J.C. Niepce ([2]), L. Normand ([3]), A. Thorel ([3]) and R. Kilaas ([4])

([1]) Centre de Recherche sur les mécanismes de croissance cristalline ([**]), Campus de Luminy, Case 913, 13288 Marseille Cedex 9, France

([2]) Laboratoire de Recherche sur la Réactivité des Solides ([***]), Université de Bourgogne, BP 138, 21004 Dijon Cedex, France

([3]) Centre des Matériaux de l'École des Mines de Paris, BP 87, 91003 Évry Cedex, France

([4]) National Center for Electron Microscopy, Materials Sciences Division, Lawrence Berkeley National Laboratory, University of California, Berkeley, CA 94720, USA

*(Received 1 July 1996, accepted 12 November 1996)*

PACS.77.84 Dy – Niobates, titanates, tantalates, PZT, ceramics, *etc.*

PACS.61.14.-x – Electron diffraction and scattering

PACS 61.16 Bg – Transmission, reflection and scanning electron microscopy (including EBIC)

**Abstract.** — The structure of ferroelectric domain walls in $BaTiO_3$ has been investigated through two complementary approaches, a global one by the fine analysis of X-ray diffraction patterns, the other essentially local *via* a quantitative image analysis method developed and applied to High Resolution Transmission Electron Microscopy images. These two original approaches converge towards a clear description of 90° walls which are shown to be a 4–6 nm wide region where the crystallographic discontinuity is accommodated by irregular atomic displacements. The results given here demonstrate that the usual structural theoretical description of walls commonly accepted for energy calculations are far too simplistic The two underlying methodologies which have been developed to carry out these approaches can possibly be applied to other ferroelectrics, but without any doubt to other systems where twins or coherent interfaces are expected

**Résumé.** — Une étude de la structure des murs de domaines ferroélectriques dans $BaTiO_3$ est réalisée à travers deux approches complémentaires : une approche globale par une méthode fine d'analyse des diagrammes de poudre de diffraction des rayons X, et une autre très locale par une méthode quantitative d'analyse des images obtenues par microscopie électronique de haute résolution. Ces deux approches originales convergent vers une description claire des murs de domaines à 90° : c'est une région large de 4–6 nm où la discontinuité cristallographique est accommodée par des déplacements atomiques irréguliers. Ces résultats montrent que la description structurale théorique communément utilisée pour des calculs d'énergies est de loin trop simpliste. Les méthodologies développées, propres à chacune des analyses structurales utilisées, peuvent être appliquées à l'étude de tout autre matériau ferroélectrique, mais aussi à tout autre matériau cristallisé où des maclages ou interfaces cohérentes sont attendues.

(*) Author for correspondence (e-mail: floquet@crmc2.univ-mrs.fr)

(**) UPR 7251 CNRS

(***) UMR 5613 CNRS

## 1. Introduction

The ferroelectric domain microstructure in $BaTiO_3$ single crystals, powders and ceramics has been observed by many techniques (Optical Microscopy [1,2], Scanning Electron Microscopy [3], Transmission Electron Microscopy [2,4–6] and recently Atomic Force Microscopy [7,8]). From these observations, descriptions of the domain microstructure has been proposed [9] showing that the domains are limited by two types of walls: the 90° and 180° ferroelectric domain walls that correspond respectively to {101} and {100} crystallographic planes. However, concerning the fine wall structure only few observations and theoretical descriptions have been published.

Thus, a limited number of researchers have carried out Transmission Electron Microscopy to study the structure and thickness of domain walls in ferroelectric or related materials [1, 5, 10–12]. Twin walls in $YBa_2Cu_3O_7$ have been observed by High Resolution Electron Microscopy (HRTEM) by Zhu *et al.* [13, 14], domain walls in $BaTiO_3$ and $LiTaO_3$ have been studied *via* the same technique by Bursill *et al.* [15], and detailed observations on $BaTiO_3$ have been reported by Tsai *et al.* [16] and Normand *et al.* [17]: nevertheless, none of these studies has given direct evidence of a precise and quantitative measurement of displacements and distortions associated with the domain walls. Using, in a TEM methods derived from holography, Zhang *et al.* have proposed a fine analysis of the domain walls structure in $BaTiO_3$ based on variations of the intensity of the polarization vector [18] that agrees with the "kink" model developed by Zhirnov. Combining HRTEM and Image Analysis, Stemmer *et al.* [19] have used a quasi-1D approach to characterize the variations of the unit cell parameter perpendicular to the wall, an approach that fits the concept of the soliton model [20]; but in either case local deformations or steps cannot be detected.

In this paper, we attempt to give a fine description of the domain wall structure by two complementary approaches. The first one is a thorough analysis of X-ray diffraction patterns, given that the XRD diagram includes fingerprints of the ferroelectric domain microstructure and particularly the domain walls. The second one is a quantitative analysis of the HRTEM images seeing that the HRTEM allows to visualize the atomic displacements at the boundary of two ferroelectric domains.

## 2. Ferroelectric Microstructure and Crystalline Structure of a Ferroelectric Material

2.1. $BaTiO_3$: A Ferroelectric Material. — At room temperature, the structure of $BaTiO_3$ is tetragonal with a $c/a$ ratio very close to 1 ($c/a = 1.01$). The material is ferroelectric because in the tetragonal cell, the positive and negative charges barycenters do not coincide, thereby inducing a spontaneous polarization parallel to the $c$-axis. To adapt itself to the cell polarization, the material is divided into ferroelectric domains characterized by a uniform polarization vector. The ferroelectric domain arrangement, antiparallel (180° domains) and perpendicular (90° domains), minimizes the overall deformation and the electrostatic energy. A schematic ferroelectric microstructure is drawn in Figure 1a.

2.2. Relation Between Crystalline Structure and Ferroelectric Microstructure. — The crystalline structure and the ferroelectric microstructure are in closely related.

- The polarization vector is parallel to the [001] axis of the cell.
- The ferroelectric domain walls are usually as sketched in Figure 1:

  - (101) or (011) twin planes for 90° domains; note that the angle between the [001] directions for two adjacent domains is exactly $2\text{arctg}(a/c) = 89\ 43°$ (Fig. 2);
  - (100) or (010) planes for 180° domains.

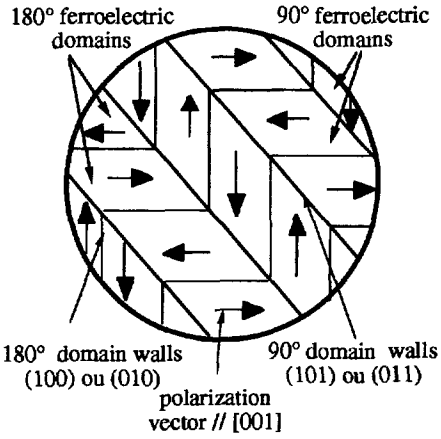


Fig. 1. — Relation between crystal structure and ferroelectric microstructure schematic ferroelectric microstructure of the area selected in the magnifying glass of Figure 3.

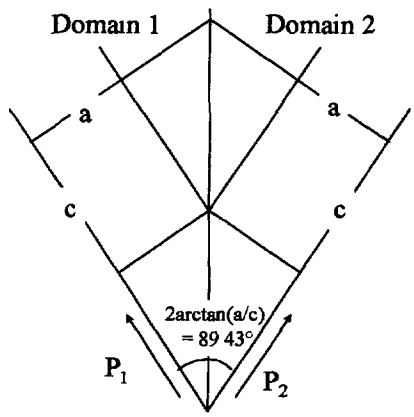


Fig. 2. — (101) twin planes for 90° domains: the true angle between the polarization directions for two adjacent 90° domains is exactly $[2\arctan(a/c)]°$.

Figure 3 shows an optical microscopy picture of a $BaTiO_3$ ceramic grain (reported by Arlt [2]): the ferroelectric microstructure appears as large strips going through the grain. Each strip is divided into two sets of narrow strips which are 90° domains. The 90° domain walls are, in one large strip, either (011) or $(01\bar{1})$ planes and in the adjacent large strips, either (101) or $(10\bar{1})$. Two adjacent large strips are separated by either (110) or $(\bar{1}10)$ planes. Note that in this optical picture, the 180° domains walls are not revealed. They would appear in the magnifying glass of Figure 3 as represented in Figure 1.

Back Scattered Electron observations by Scanning Electron Microscopy (SEM) of free surfaces of a sintered polycrystalline sample gives complementary details on the general domain configuration; in such SEM images (Figs. 4a and 4b) where the contrast is crystallographic and due to the slight misorientation between two adjacent domains, one can observe a typical configuration on {100} growth terraces. Our systematic SEM study of the general arrangement of domains corroborates perfectly what is proposed in the literature.

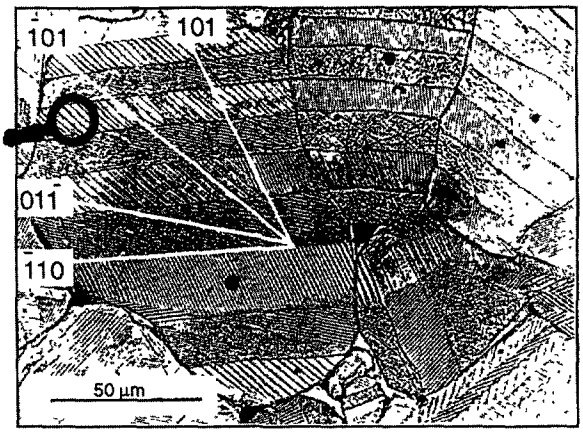


Fig. 3. — Optical microscopy picture of a $BaTiO_3$ ceramic grain [2].

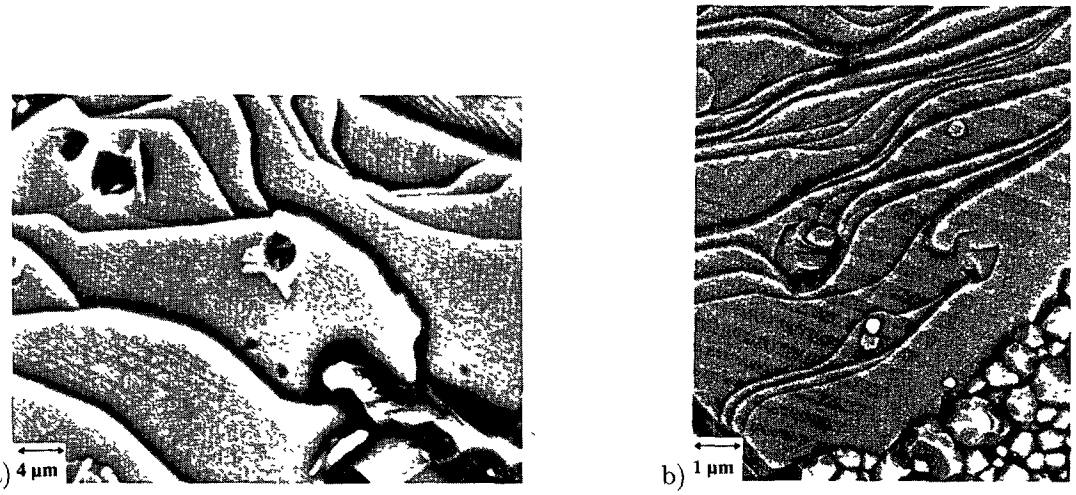


Fig 4. — SEM back scattered images showing a typical domain configuration on {100} growth terraces; the "herring-bone" structure is clearly visible in (a).

Because of the relationships between the crystalline structure and the ferroelectric microstructure, a $BaTiO_3$ grain looks like a multiple twinned crystal. The powder XRD diagram of $BaTiO_3$ should contain the fingerprints of this ferroelectric microstructure. Thus, a full and accurate XRD study was carried out in order to fully describe the ferroelectric microstructure.

## 3. Fingerprints of the Ferroelectric Microstructure Revealed in the $BaTiO_3$ XRD Diagram

In order to reveal these fingerprints, a simple solution consisted in varying the ferroelectric domain microstructure in a known manner while recording the XRD diagrams. After a brief presentation of the $BaTiO_3$ XRD diagram, it will be shown how this diagram evolves, on the one hand, by applying an increasing electric field to the ceramic material and, on the other hand, by progressively heating the powder material through the Curie temperature.

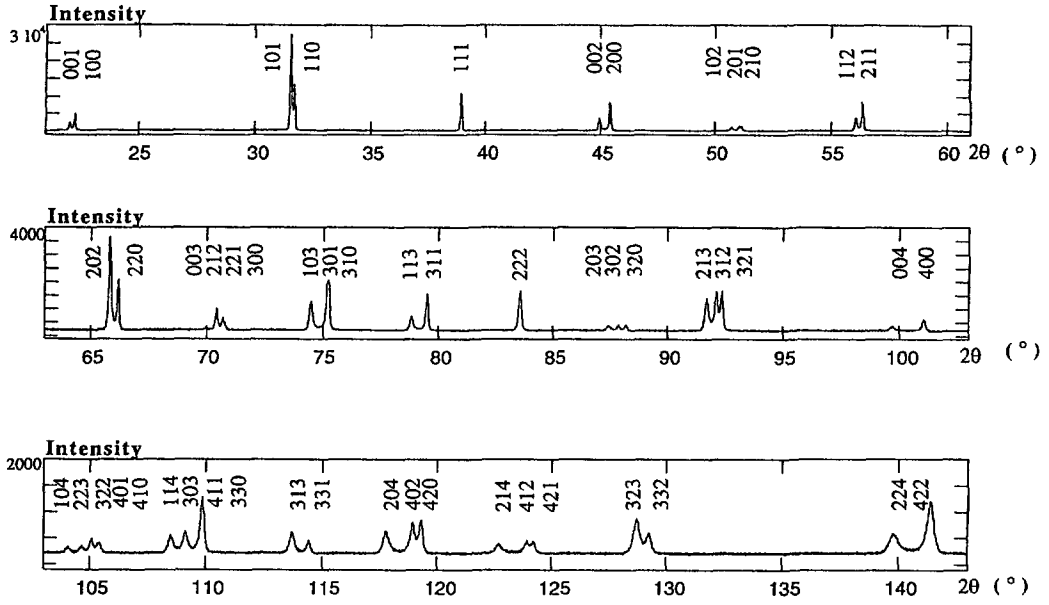


Fig. 5 — Indexed $BaTiO_3$ XRD diagram.

3.1. $BaTiO_3$ XRPD DIAGRAM. — The powder XRD diagram of tetragonal ferroelectric $BaTiO_3$ is represented in Figure 5. As for a tetragonal structure material with $c/a$ ratio close to 1, the diagram is composed of single lines and of doublets and triplets.

The single lines are symmetrical as for an "usual" crystalline material. By contrast, the doublets and triplets have very particular profiles. The doublet profiles could be described in two different ways:

- the sum of two dissymmetrical lines, with the dissymmetry inside the doublet (Fig. 6a)
- the sum of two symmetrical lines with specific diffracted intensities in the two lines and of a particular diffracted intensity between the lines (Fig. 6b).

The study of the XRD diagram evolution as a function of physical factors, such as the electric field and the temperature, allowed to highlight two fingerprints of the ferroelectric domain microstructure,

- the relative intensities of two lines of a doublet,
- the symmetrical profiles of the simple lines. It also confirmed that the particular profiles of doublets and triplets are domain microstructure fingerprints.

3.2. RELATIVE INTENSITY OF THE ASSOCIATED LINES: POLARIZATION STATE OF THE MATERIAL. — *In situ* XRD experiments allowed to record the XRD diagram of a ceramic disk of $BaTiO_3$, when an electric field is applied perpendicularly to it. An experimental device was specially built for this purpose. Thus, XRD diagrams of the $BaTiO_3$ ceramic were registered as a function of the applied electric field.

Why apply an electric field to a ceramic? In order to force the material to adapt itself to this external strain by modifying its domain microstructure and thus to record the possible modifications of the XRD diagram.

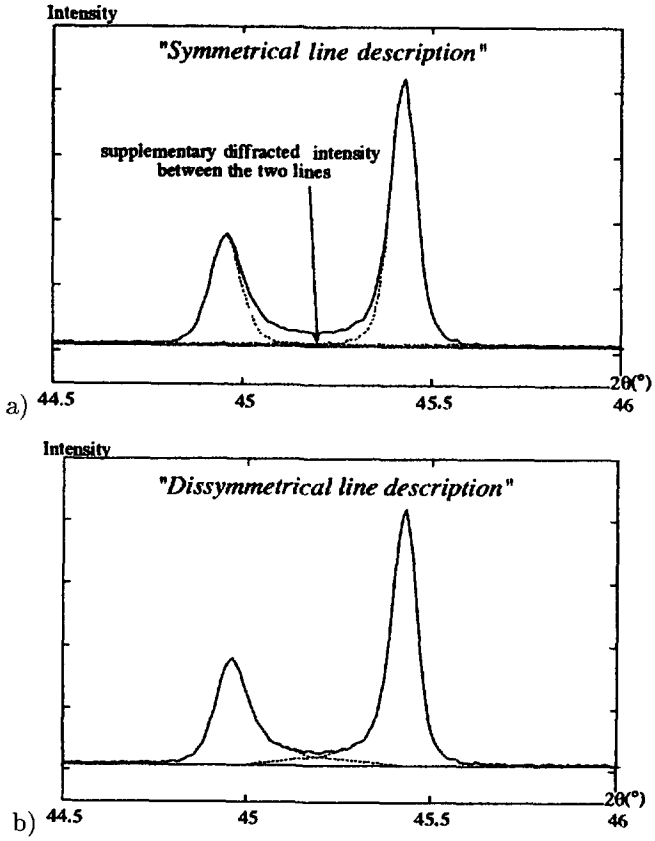


Fig. 6. — Two ways for the doublet line description in the $BaTiO_3$ XRD diagram: a) dissymmetric description, b) symmetric description.

The electric field effect is shown in the XRD diagram by an evolution of the relative intensities of the diffraction lines. For example in the 002/200 doublet, when the electric field is increased, the intensity of the 002 line increases at the expense of the 200 line (Fig. 7). This can be explained by the motion of the ferroelectric domains walls inducing the growth of the domains with a polarization vector closest to the electric field. The polarization direction being parallel to the $c$-axis, the (001) plane families proportionally increase at the expense of the (100) plane families (Fig. 8). The relative intensities of the doublet lines express the polarization state of the material [21].

The curve $R = f(E)$ (Fig. 8), obtained from the diffracted intensity measurements, is compared to the schematic first polarization curve $P/P_s = f(E)$.

Electric polarization measurements and XRD do not analyze the polarization state on the same way:

- the electric measurements consider the whole sample volume, with all the grains (whatever their orientation), with all the domains (180° and 90°);

- XRD considers only the surface (a few mm) and only some grains (that are in diffraction angular position) and two anti-parallel domains (180°) are not distinguished.

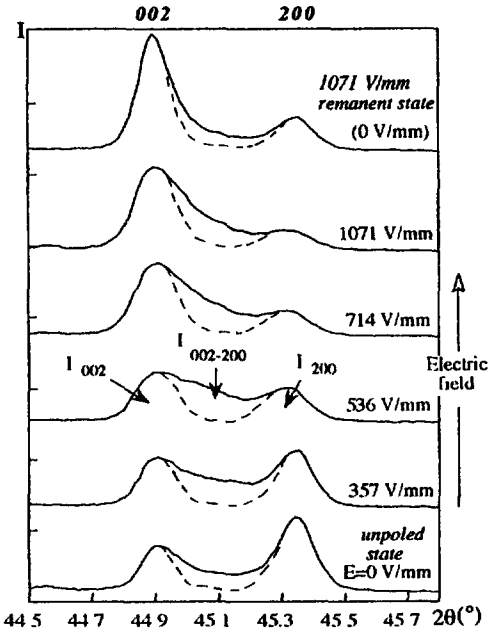


Fig. 7. — Evolution of the 002/200 doublet as the electric field increases.

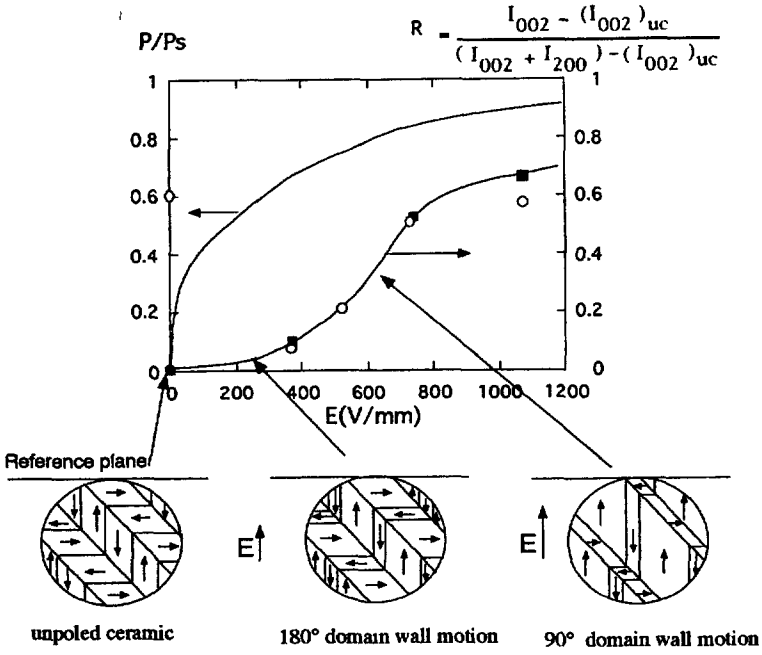


Fig. 8. — Comparison between a diagrammatic relative polarization $P/P_s$ curve and the $R$ curve obtained by X-ray diffraction measurements. Corresponding schematic evolution of the ferroelectric domain microstructure.

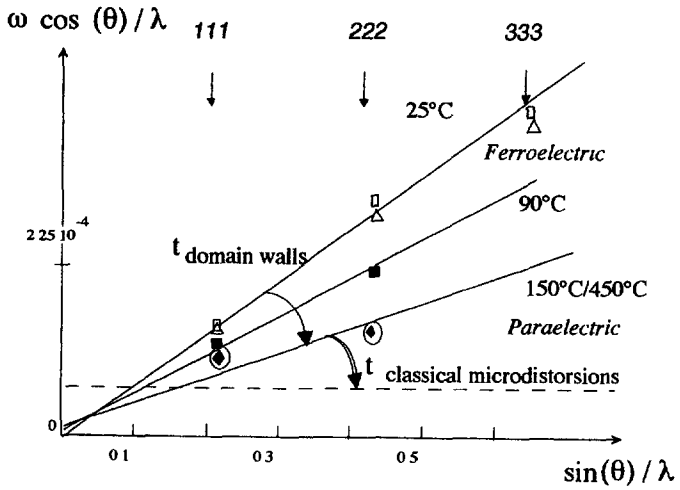


Fig. 9 — Experimental proof of the domain wall contribution as lattice microdistorsions to the line broadening

The comparative interpretations of the $R$ and $P/P_s$ curves allow to characterize the domain wall motion under the influence of the electric field. The 180° domain wall motion occurs for a very low value of the electric field for which $R = 0$, whereas the 90° domain walls move for a higher value of the electric field corresponding to $R > 0$.

This study shows that X-ray diffraction could be, when associated with electric measurements, a quantitative tool to distinguish the energies required for 90° and 180° domain wall motion under an external strain effect.

3.3. Single Line Profiles: Domain Walls as Microdistortions. — Contrary to the double lines, the profile of the single line is well defined. The study of the *hhh* line broadening with temperature, through a Williamson and Hall [22] plot should bring qualitative data on the crystallite size (coherent diffraction size) and lattice microdistortion of the material. The W-H diagram consists in a straight line with the origin ordinate leading to the mean apparent crystallite size and the slope to the mean apparent defect ratio in the direction perpendicular to the *hkl* planes being considered.

The XRD diagrams were collected in LURE using the D23 diffractometer [23]. The results are presented in a W-H plot of the *hhh* lines as a function of the temperature (Fig. 9).

As the temperature increases up to the phase transition temperature $T_C$, the slope decreases. For temperatures above $T_C$ ($T_C < T < 450$ °C), there is no more evolution of the slope.

At low temperatures ($T < T_C$), the decrease of the broadening cannot to be explained by a classical lattice distortion relaxation (in such a case, this relaxation will not stop at $T_C$). But then, it is possible to explain this decrease by the relaxation of particular microdistortions: the ferroelectric domain wall. As the tetragonality decreases with temperature, the domain walls are less and less a defect given that the lattice misfit between two adjacent domains is decreasing (Fig. 10). The contribution of the domain wall to the slope ($S_{dw}$) decreases, to finally disappear at $T_C$ when the $BaTiO_3$ lattice becomes cubic.

For $T_C < T < 450$ °C, there are no ferroelectric domains left and the value of the slope represents only classical microdistortions ($S_{ld}$). Such an interpretation is consistent with the broadening observed when cooling back to room temperature. Due to the fact that

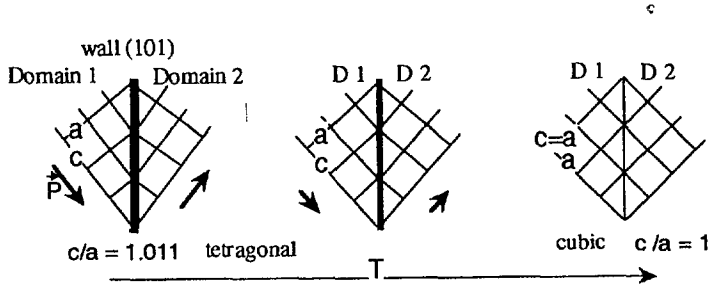


Fig. 10. — Diagrammatic representation of a domain wall between two 90° adjacent ferroelectric domains as a function of temperature: increasing the temperature, decreasing the particular lattice distortions that are the ferroelectric domain walls.

ferroelectricity is reversible, the slope and the apparent defect ratio due to the domain walls return to their initial values.

Note that in this study, the origin ordinate remains approximately equal to zero and has no real significance. This is due to the large grain size; thus the approximation of the infinite size crystal is valid all along this study.

The study of the *hhh* line broadening by this method as a function of the temperature, shows that the ferroelectric domain walls contribute to the *hhh* line width. This result proves that the ferroelectric domain walls act as particular lattice microdistortions.

### 3.4. Particular Profiles of Doublets and Triplets: Stress State of the Ferroelectric Domain Microstructure

*3.4.1. Influence of an Electric Field on a $BaTiO_3$ Ceramic.* — The most visible modification of the XRD diagram as a function of electric field is the evolution of the intensities of the lines (3.2.). However, a thorough study shows that the particular profile of doublet or triplet, due to a supplementary diffracted intensity between the lines, evolves with the electric field (Fig. 7).

This particular intensity, denoted $I_{002-200}$, has been evaluated by assuming a symmetric profile of each line with respective intensities $I_{002}$ and $I_{200}$ (Fig. 6b).

The integrated intensity ratio of the two lines ($I_{002}/I_{200}$) increases with the electric field ($E$) whereas the relative intensity between the 002-200 double lines ($I_{002-200}/(I_{002} + I_{200})$) goes through a maximum (Fig. 11). The curve $I_{002-200} = f(E)$ is similar to the derivative of the curve $I_{002}/I_{200} = f(E)$. Its maximum ($I_{002-200}/(I_{002} + I_{200}) = 0.85$) matches the maximum of transformation rate of the 90° ferroelectric domains ($I_{002}/I_{200} = 2$). As the evolution of the microstructure is at its maximum under the electric field effect, the diffracted intensity between the double lines is at its maximum too. Thus, that particular diffracted intensity well characterizes the ferroelectric domain microstructure and is related to the stresses induced by the domain wall motion.

*3.4.2. Influence of the Temperature on a Powder.* — Heating a $BaTiO_3$ powder above its tetragonal-cubic transition temperature ($T_C \approx 120$ °C), is an other way to modify and finally to remove the ferroelectric domain microstructure.

The XRD diagrams were recorded at different temperatures, from room temperature up to 350 °C (Figs. 12, 13). As the temperature increases up to $T_C$,

- the 002 and 200 line positions get closer to the cubic 002 line position;
- the ratio $I_{002}/I_{200}$ does not change;
- the intensity $I_{002-200}$ between the double lines decreases a little bit.

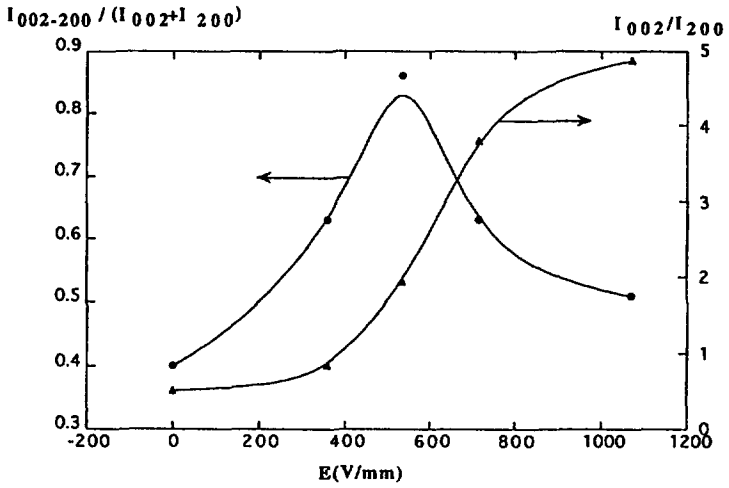


Fig. 11. — Comparison between the 002 and 200 line intensities and the particular intensity between the doublet lines as a function of electric field

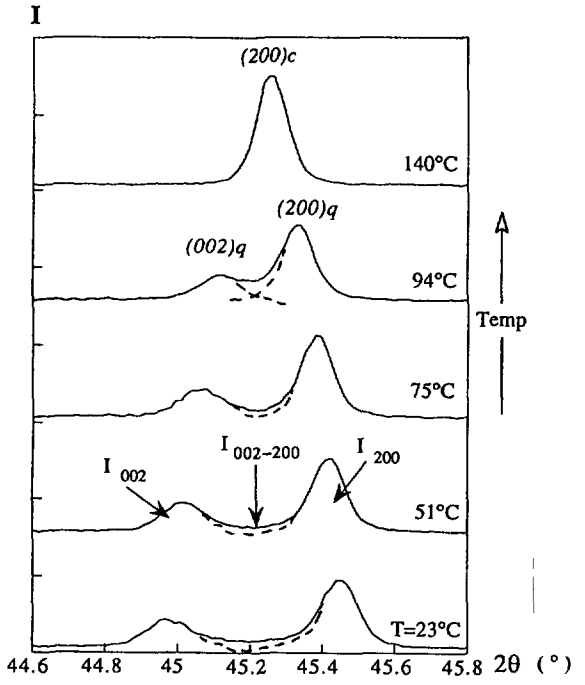


Fig. 12. — Evolution of the 002/200 doublet lines as a function of temperature.

As the tetragonality decreases with temperature, the microstructure progressively vanishes. Thus, this diffracted intensity between the two lines of a doublet should again be related with the ferroelectric domain microstructure.

Note that this particular intensity is more significant in the ceramic than in the powder

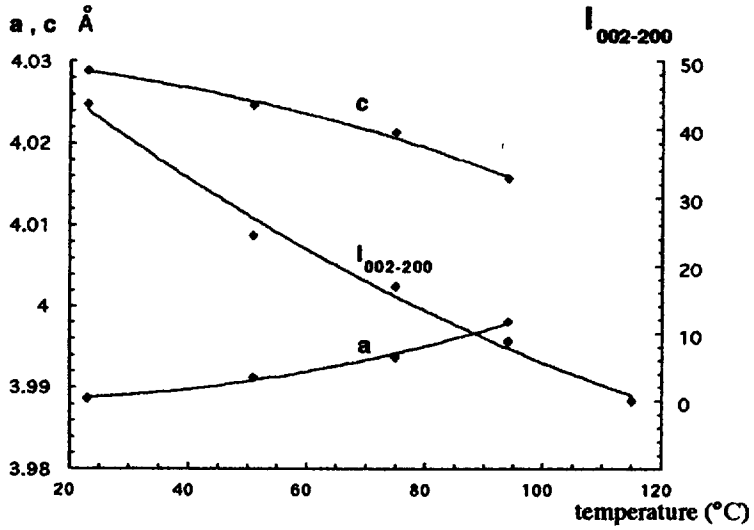


Fig. 13. — Comparison between the lattice parameter evolution and the particular intensity between the doublet line evolution as a function of temperature.

(Figs. 7, 12), probably due to the mechanical and electrostatic interactions of each grain of the ceramic with its neighbours [24]. This difference between the "stressed" microstructure of a grain in a ceramic and the "free" microstructure of the grain in a powder explains the difference in the diffracted intensity between the two double lines.

3.5. Particular Profiles of Doublets and Triplets: a Coherent Contribution in the Whole Diagram. — The particular diffracted intensity between the (002/200) doublet is related to the ferroelectric domain walls. As a wall cuts every crystalline plane except itself, the effect of the domain walls should appear in all *hkl* lines and, moreover, their contribution would have to be coherent in the whole diffractogram.

The XRD diagram was recorded using a $\theta-2\theta$ goniometer (Siemens D 500) [25]. A coarse grained $BaTiO_3$ powder, with a narrow grain size distribution (1−2 $\mu$m), has been used in order to get well separated lines of doublets and triplets.

Two complementary ways of investigation were performed in order to describe the particular diffracted intensity between the lines.

*3.5.1. Dissymmetrical Line Description.* — In this first way of investigation, a doublet or a triplet is considered as a sum of two or three dissymmetrical lines. Each line of the whole diagram was fitted to a dissymmetrical Pearson VII function without any physical criterion. The Siemens Profile software is used. The line dissymmetry is represented by the ratio of the integrated width of the left half over the integrated width of the right half of the line. This ratio, noted $f$, is greater than 1 if the line is left dissymmetrical, smaller than 1 if the line is right dissymmetrical, and equals to 1 if the line is symmetrical. Aberrant fits, occurring for very mixed lines, are excluded.

To give a synthetic view of the results, a stereographic projection is used. The (001) stereographic projection (Fig. 14a) shows the [011] and [101] meridians and their equivalents intersecting in (111) and equivalents. They define three areas that correspond to the lines splitting

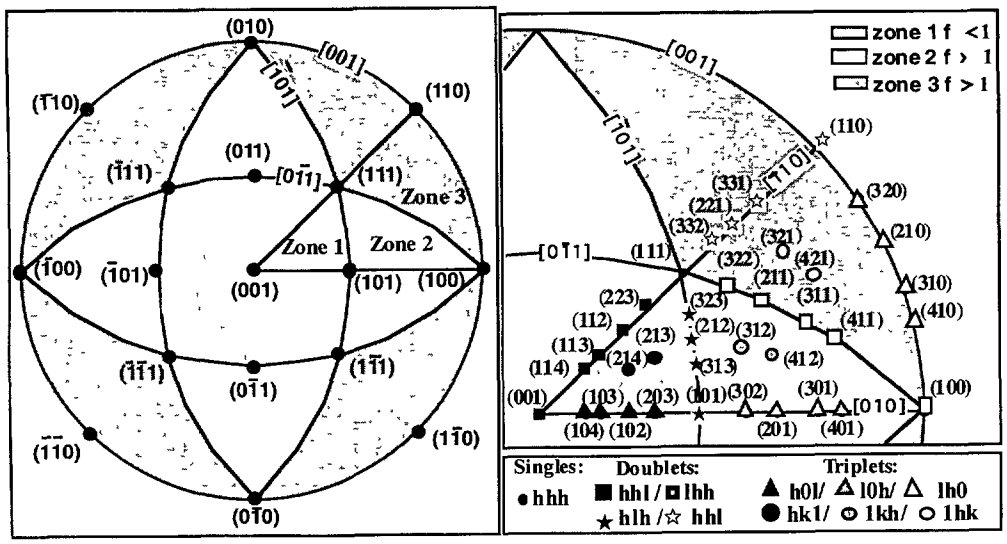


Fig 14. — Dissymmetry factor of the diffraction lines represented in the (001) stereographic projection of the $BaTiO_3$ structure: a) whole projection; b) focused projection of the non equivalent *hkl* lines

through the cubic–tetragonal transformation: one line of the cubic structure splits in three lines of the tetragonal structure.

Figure 14b focuses on all non equivalent *hkl* lines. The doublet lines are on the $[1\bar{1}0]$, $[0\bar{1}1]$, $[\bar{1}01]$ meridians. The two lines of a *hhl/lhh* doublet are on $[1\bar{1}0]$ and $[0\bar{1}1]$ meridians respectively. The two lines of a *hlh/hhl* doublet are on $[\bar{1}01]$ and $[1\bar{1}0]$ meridians respectively. The lines on the $[1\bar{1}0]$ meridians have half the intensity of the lines on the two other meridians due to the difference of multiplicity.

The *h0l/l0h/lh0* triplet lines are on the [010] and [001] meridians. The first one is on the [010] between (001) and (101). The second one is on the [010] between (100) and (101). The third one is on the [001] between (100) and (110). Each line of the *hkl/lkh/lhk* triplet is in one of the three areas. All the triplet lines are of same intensity because they have the same number of equivalents.

The dissymmetries $f$ of the lines are reported in Figure 14. The right dissymmetrical lines ($f = 0.6$ to 0.8) are in the area 1, the nearly symmetric lines ($f \sim 1$) are in the area 2 and the left dissymmetrical lines ($f = 1.2$ to 1.4 ) are in the area 3. These results prove that the dissymmetry of all the diffractogram lines is coherent with the $BaTiO_3$ tetragonal structure.

For each doublet, the ratio of the first line dissymmetry ratio over the second line dissymmetry ratio ($f_1/f_2$) is nearly constant. This proves that the dissymmetry is the same whatever the doublet. Note that, in a doublet, the first line is right dissymmetrical whereas the second is left dissymmetrical. This result is in agreement with the supplementary diffracted intensity observed between the two lines of a doublet.

For the triplets, the first line is right dissymmetrical, the second is nearly symmetrical and the third is left dissymmetrical. This observation evidences that a triplet must be analyzed as three doublets by associating the lines pairwise: the first line of the triplet is always right dissymmetrical because its counterparts are the second and the third lines; the third one is

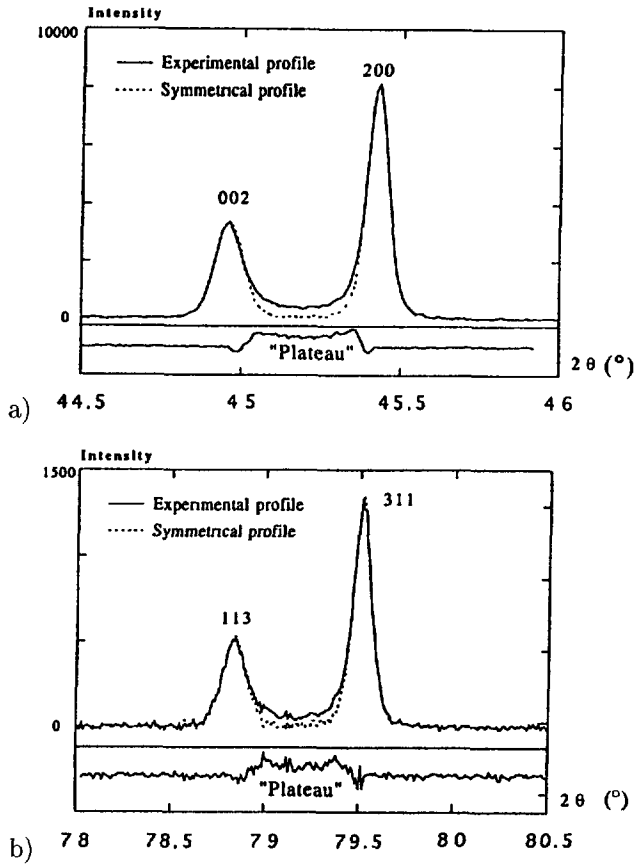


Fig 15. — Manifestation of a "plateau" between the lines of a doublet.

always left dissymmetrical because its counterparts are the first and the second lines; the second one is always nearly symmetric because it is left dissymmetrical with its left counterpart (the first line) and right dissymmetrical with its right counterpart (the third line).

*3.5.2. Symmetrical Line Description*

3.5.2.1. Manifestation of a "Plateau" Between the Lines of a Doublet. — In the second way of investigation, the profile of a doublet is considered as a sum of two symmetrical lines and of a supplementary diffracted intensity between the lines. The left part of the left line and the right part of the right line are well defined. Two calculated symmetrical lines are built by "symmetrizing" the two well defined half profiles. The two symmetrical resulting lines are subtracted from the experimental profile of the doublet. The difference looks like a rectangular function called a "plateau", with the symmetrical line maxima as ends. All the doublets can be described with this model (Fig. 15).

The plateau intensity ranges between 8 and 12% of the doublet intensity. The 4% intensity error comes from the lack of precision in the $2\theta$ position choice of the line maxima. A small error in the maxima choice induces a important error in the plateau intensity. Whatever the doublet, the plateau intensity is nearly constant with respect to the doublet intensity. The plateau intensity has an average value of 10% of the doublet intensity.

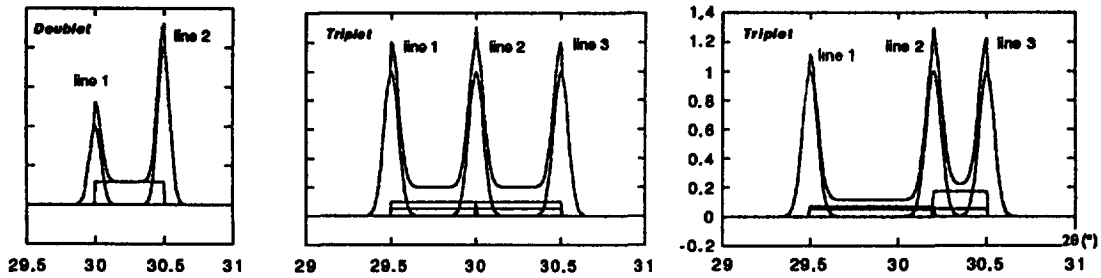


Fig. 16. — Plateau model for the doublets (a) and the triplets (b, c).

The doublet intensity could be expressed by: $I_{\text{doublet}} = (I_{hhl} + I_{lhh} + p_{\text{d}})$ with $I_{lhh} = 2I_{hhl}$ if $h < l$ and $I_{hhl} = 2I_{lhh}$ if $h > l$ and $p_{\text{d}}$ = doublet plateau intensity, with $p_{\text{d}} = p_{\text{dmax}} \times \Delta 2\theta$, $p_{\text{dmax}}$ being the intensity maximum of the plateau and $\Delta 2\theta$ being the angular difference between the two lines. Thus, as observed in Figure 15, the intensity maximum of the plateau depends on the angular difference between the two lines.

3.5.2.2. "Plateau" Model Applied to the Triplets. — As shown previously, a triplet is made of two by two associated lines, thus the plateau model can be applied in the same way. The triplet intensity could be expressed by: $I_{\text{triplet}} = (I_{hkl} + I_{lkh} + I_{hlk} + p_{\text{t}})$. For the sake of conciseness, $I_{hkl} = I_1$, $I_{lkh} = I_2$, $I_{hlk} = I_3$, with $I_1 = I_2 = I_3$. $p_{\text{t}}$ is the supplementary integrated intensity between all the lines taken pairwise:

$$p_{\text{t}} = p_{12} + p_{23} + p_{13} \text{ with } p_{12} = p_{12\text{max}} \times \Delta 2\theta_{12},\ p_{23} = p_{23\text{max}} \times \Delta 2\theta_{23},\ p_{13} = p_{13\text{max}} \times \Delta 2\theta_{13}.$$

Since a doublet is a particular triplet, the supplementary intensity between the lines is assumed to be the same in a doublet and a triplet: $p_{\text{t}}/I_{\text{triplet}} = p_{\text{d}}/I_{\text{doublet}}$ and $p_{12} = p_{23} = p_{13} = p_{\text{t}}/3$. Thus, in a triplet, the three plateau maxima will have different values, depending on the angular position of the middle line (Fig. 16).

The dissymmetry approach has shown that the doublet and the triplet could be analyzed in the same way. No $(hkl)$ plane family seems to be particular. This analysis well proves that the character of the profile is coherent in the whole diagram. The plateau model confirms this coherence and allows to bring a clear distinction between the diffractogram particularities of such a tetragonal ferroelectric material from the diffractogram of a classical tetragonal material without microdistortion.

3.6. "Plateau" Model and Structural Description of the 90° Domain Walls. — By these two approaches the particular profiles could be interpreted by an interplanar distance distribution in the material. The plateau model shows that this distribution is constant and the interplanar distance varies between the interplanar distances of the two counterpart planes. The two counterpart planes could be deduced from each other by a mirror symmetry about (101) or (011) planes. Also, two 90° ferroelectric domains correspond to each other by the same mirror symmetry planes that are the boundaries between two 90° domains.

Thus, the symmetrical lines come from the diffraction of the ferroelectric domains whereas the plateau comes from a misfit boundary area between them. This interpretation suggests that the 90° ferroelectric domain walls are not twin planes but misfit boundary area. The thickness of these walls is proportional to the plateau intensity. The wall is built of crystalline

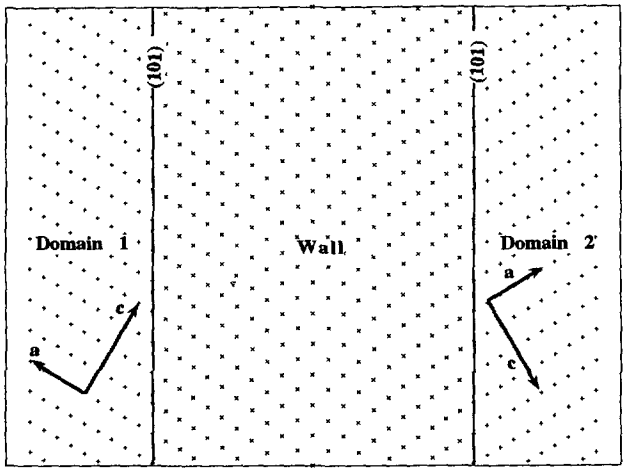


Fig. 17. — Plateau model and evolution of the crystalline lattice inside a 90° domain wall.

planes which interplanar distance varies from the *hkl* interplanar distance in one of the 90° domain to the *lkh* or *hlk* counterpart distance in the adjacent domain (Fig. 17).

## 4. Quantitative High Resolution TEM Image Analysis

A transmission electron microscopy study has been carried out in order to cross-check by a more localized investigation the approach by X-ray diffraction described above. First, conventional TEM and electron diffraction have been performed to obtain an overall characterization and localization of the domain wall structure as well as a long range measurement of the twin angle in our material; then an original methodology based on the quantitative analysis of digitized HRTEM images has been developed in order to obtain a precise evaluation of atomic displacements in the immediate vicinity of 90° walls [26].

4.1. Experimental — Sintered polycrystalline $BaTiO_3$ was cut into 3 mm disks, mechanically polished, dimpled and ion milled to obtain a sample transparent to the electron beam Observations have been carried out at 800 kV on the Jeol Atomic Resolution Microscope (ARM1000), and at 200 kV on a Jeol 200CX and a TopCon 002B. Samples observed at 800 kV were carbon coated to prevent from charging under the electron beam. HRTEM original negatives were scanned by use of a 6000 element CCD LeafScan 45 scanner connected to a Macintosh microcomputer; 1024 × 1024 or 2048 × 2048 pixels digitized images were obtained and analyzed through the Digital Micrograph software. Digitization must be carried out without any interpolation and must allow the description of an atomic column with $8^2$ to $10^2$ pixels. The existing methods such as "template matching" has been proved not to be accurate enough to detect atomic displacements at domain walls in our material. The calculation of the atomic displacements was then carried out by means of specific subroutines which have been developed as "custom functions" derived from the "peak finding" technique.

4.2. Conventional TEM Images. — Figure 18a shows a typical view of 90° domain walls in a $BaTiO_3$ grain observed with a transmission electron microscope at a low magnification.

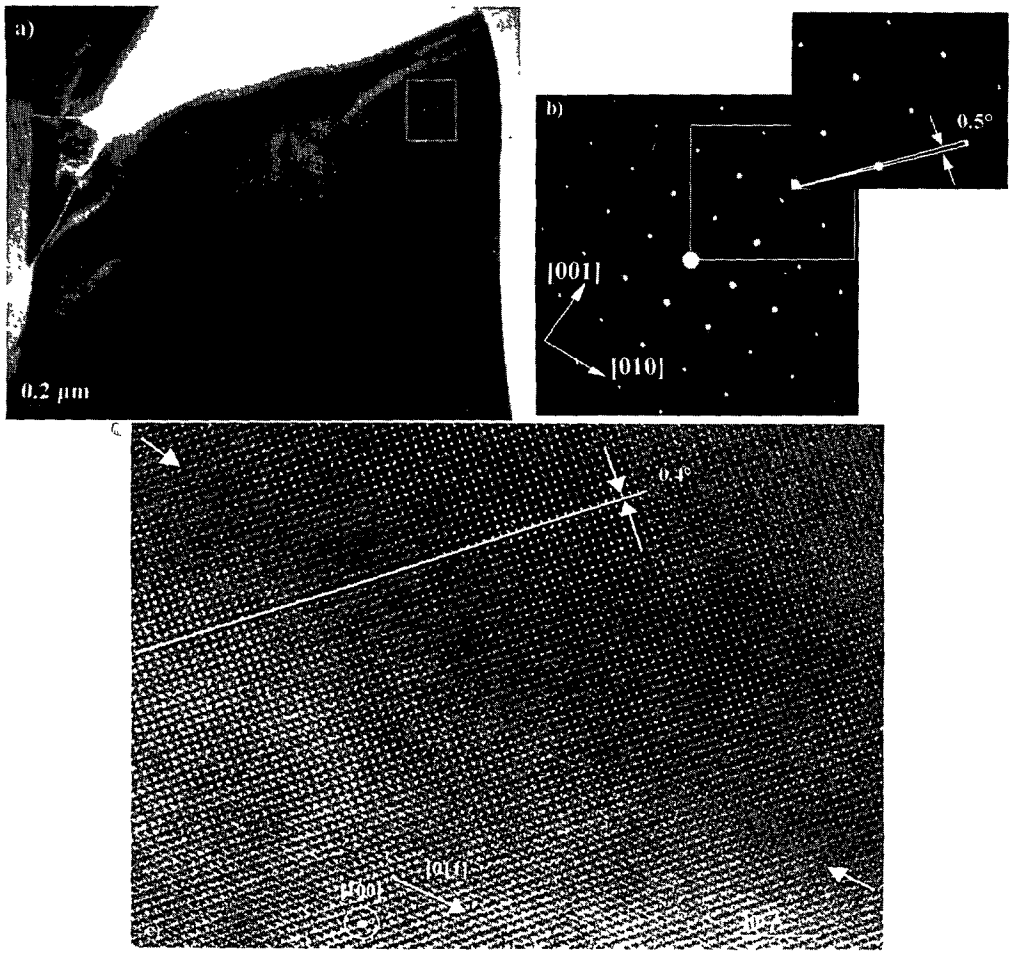


Fig. 18 — a) Low magnification TEM image taken along a ⟨100⟩ zone axis showing 90° domain walls; b) Selected Area Diffraction Pattern of the zone indicated by a white frame in Figure 16a, enlargement of a part of the SADP to enhance the splitting of the (011) spots, c) High Resolution Transmission Electron Microscopy imaging of the same selected area where the angle between the (001) planes across the wall is indicated.

For ⟨100⟩ type orientations, two different diffraction patterns are found.

- for the so-called $a-a$ walls (when the $a$-axis is parallel to the electron beam for both grain), the habit plane is parallel to the beam and the splitting of the reflections $(0kk)$ and $(0k-k)$ is maximum, then the true long range twin angle can be measured and reaches 0.5° as can be seen in Figure 18b; this value is consistent with what is expected from the tetragonal parameters obtained from X-ray diffraction and from general considerations of crystallographic models for twinning;

- for the so-called $a-c$ walls (when the beam is parallel to the $a$-axis of one domain and to the $c$-axis of the other) the habit plane is oriented 45° from the electron beam direction and is associated with a fringe contrast; estimation of the twin angle from diffraction patterns is then not straightforward.

4 3. STANDARD ANALYSIS OF HRTEM IMAGES. — Figure 18c shows a detail of the 90° walls seen in Figure 18a imaged by the High Resolution imaging technique; one can observe that going from diffraction contrast to phase contrast diminishes the intrinsic contrast of the wall, which is in certain cases extremely difficult to locate. The 0.4° twin angle is nevertheless found, even if the measurement is less easy than in the diffraction pattern. But a 4–5 nm wide slight diffuse dark contrast (about 10 unit cells) associated with the wall can be clearly seen. This has been observed in all HRTEM images of domain walls that have been taken.

Furthermore we systematically observed in $BaTiO_3$ a strong degradation of the spatial resolution of the HRTEM images in the immediate vicinity of the walls. Since the distance between the Ba atoms and the Ti atoms is very close to 0.2 nm. well within the excellent capability of the microscopes we have been using (which resolution ranges from 0.16 for the ARM to 0.19 nm for the Topcon 002B) we could expect routinely to separate the two metallic atoms of the structure. We only succeeded to record such images far away from any walls as can be seen in Figure 18c where the spatial resolution is better than 0.2 nm, allowing thus the Ba and Ti lattices to be clearly seen whereas it is at best equal to 0.4 nm close to a wall.

Numerical diffractograms obtained from a Fourier analysis on 256 × 256 pixel areas (about 24 × 24 unit cells) centered on 90° walls reveal diffraction spots that are much more diffuse than when taken away from the vicinity of a wall. Diffractograms taken from wider areas show in addition the splitting due to the superimposition of the patterns relative to the two domains as in the electron diffraction.

From these preliminary HRTEM observations, it can be inferred that the diffuse contrast associated with the 90° walls could originate from either local distorsions of the $BaTiO_3$ lattice or the modification of the phase of the incoming electron wave by the local polarization. Since the respective influence of these two contributions cannot be clearly distinguished on the observed contrast, and owing to the fact that structural distortions have immediate consequences on the local polarization, we assumed in this paper that the contrast associated with the walls in HRTEM images was essentially due to local displacements of metallic ions in the $BaTiO_3$ lattice.

## 4.4. QUANTITATIVE ANALYSIS OF HRTEM IMAGES

*4.4.1. Principles and Experimental Conditions.* — We developed "custom functions" derived from the "peak finding" method in order to quantify the atomic displacements of metallic ions associated with the specific contrast of 90° walls in HRTEM images. The long term goal of such an approach, well beyond the frame of this paper, is the evaluation of the behavior of the polarization vector across the wall and consequently the direct calculation of the wall energy.

The "peak finding" method is based on the search of local maxima of intensity in a digitized image; this is particularly easy in a HRTEM image provided that an atomic column is described by a sufficiently large enough number of pixels. Since only the cell distortion is looked for, it is not necessary to restrain the imaging conditions to the case where a column of atoms is only white, or only dark: the important point is that the images display a sharp periodicity, black or white, corresponding to the cations lattices. The Scherzer defocus imaging conditions will possibly be chosen for it corresponds to the best stability of the microscope contrast transfer function over a wide range of spatial frequencies, leading then to the same contrast for the different types of cations columns in the $BaTiO_3$ lattice (see Fig. 19 for two different zone axes). Even though it is not of prime importance to know whether atoms are black or white, it is nevertheless absolutely essential to check that the experimental conditions (defocus, thinness) remain stable within the whole area under considerations, *i.e. there is no* bending of the foil or differential thinning. Usually the areas which are analyzed are small enough to assume that

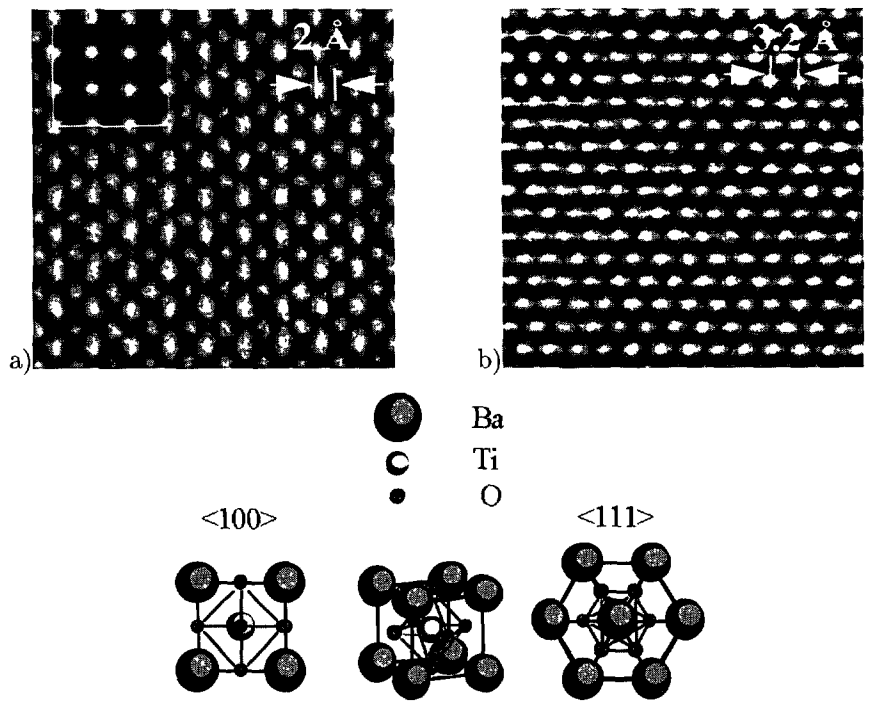


Fig. 19. — HRTEM images of $BaTiO_3$, corresponding contrast simulations on the upper left corners; a) along ⟨100⟩; b) along ⟨111⟩.

such artifacts remain negligible and we have tried to study walls oriented perpendicular to a hole in the sample in order to get rid of any thickness gradient across the wall (see Fig. 18a). Defocus and thickness for the HRTEM images are to be carefully cross-checked in association with contrast simulations.

Once the "peak finding" technique was adapted to the requirements of the HRTEM images of the $BaTiO_3$ lattice, we carried out the different sequences of our "custom function" based on the systematic comparison between a perfect lattice, created from a non perturbed region of the HRTEM image, and the real lattice taken from the general view including the 90° wall: taking into account pixelation noise as well as random displacements, the software translates and superimposes automatically the ideal perfect lattice to the real distorted one by steps of one reticular distance. For each step it makes the calculation of the translation vector corresponding to the position of the centers of weight for both superimposed cells. Results are given under the shape of maps where these displacement vectors are plotted, the direction and modulus of the vectors being representative of the direction and intensity of the atomic displacements. The accuracy then obtained is better than 0.01 nm. The validity of the technique has been verified when applied to a large 100 × 100 nm area free of any wall: no significant atomic displacement was found.

*4.4.2. Results.* — Two examples of such a quantitative treatment are presented in Figure 20a and 20b where one can see HRTEM images of 90° domains observed along a ⟨100⟩ direction; the walls (indicated by white arrows) are barely located in the experimental images, but are strongly revealed in the atomic displacement vector plots.

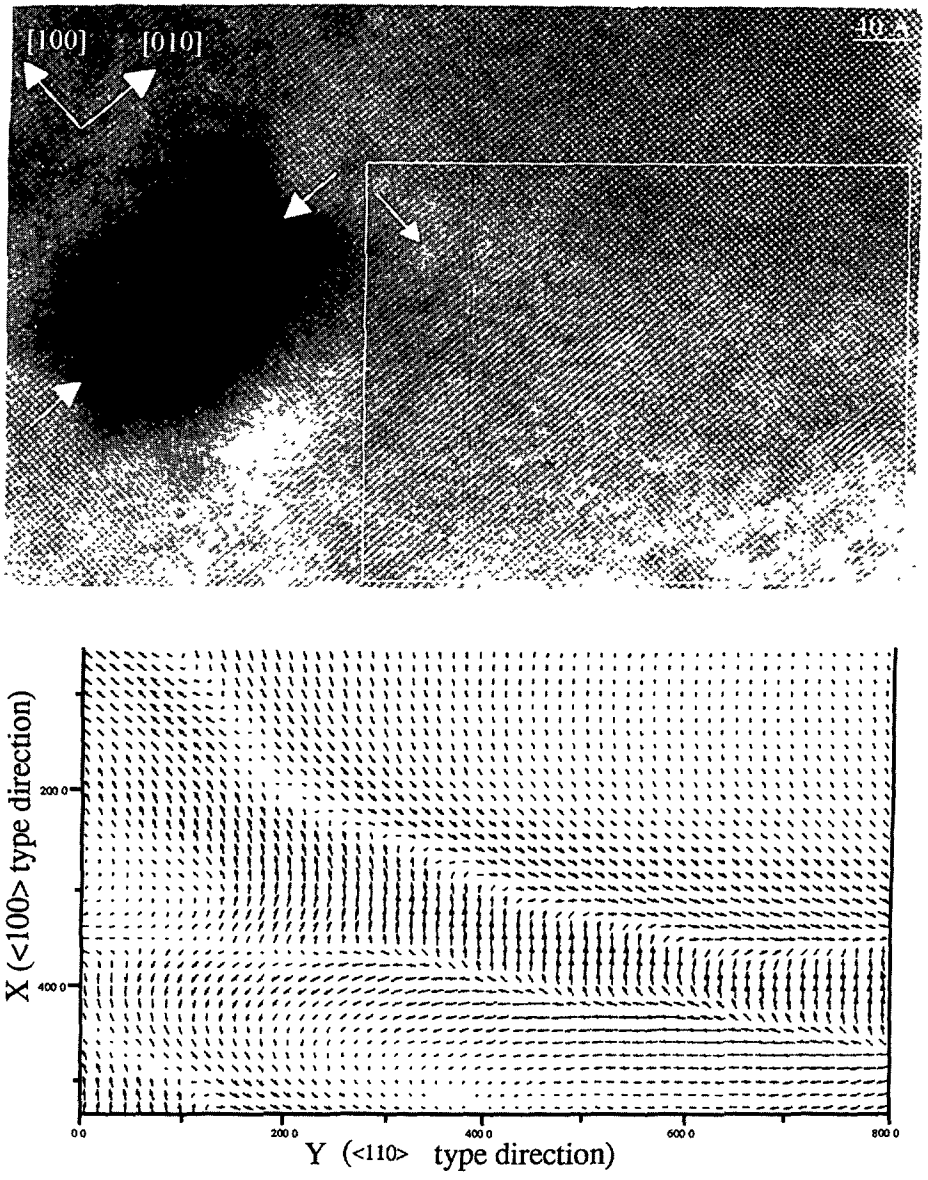


a)

Fig. 20. — HRTEM images of 90° domain walls and the corresponding atomic displacement vector plots, a) the map corresponds to the framed area in which the wall is arrowed; the defect on which the wall is pinned is also indicated by white arrows; the perfect lattice has been generated from the non distorted area in the upper right corner of the HRTEM image; b) the wall is hardly seen on the HRTEM image, it appears clearly on the map where {100} are given evidence.

The first and straightforward consequence brought by these 2D-displacement maps is a direct and local confirmation of the structural interpretation given by the X-ray diffraction fine analysis earlier in this paper: 90° domain walls in $BaTiO_3$ can no longer simply be considered as twinning habit planes, but must be described as an area of a *certain thickness* ($\sim$ 5 nm) across which the cell parameters vary more or less continuously.

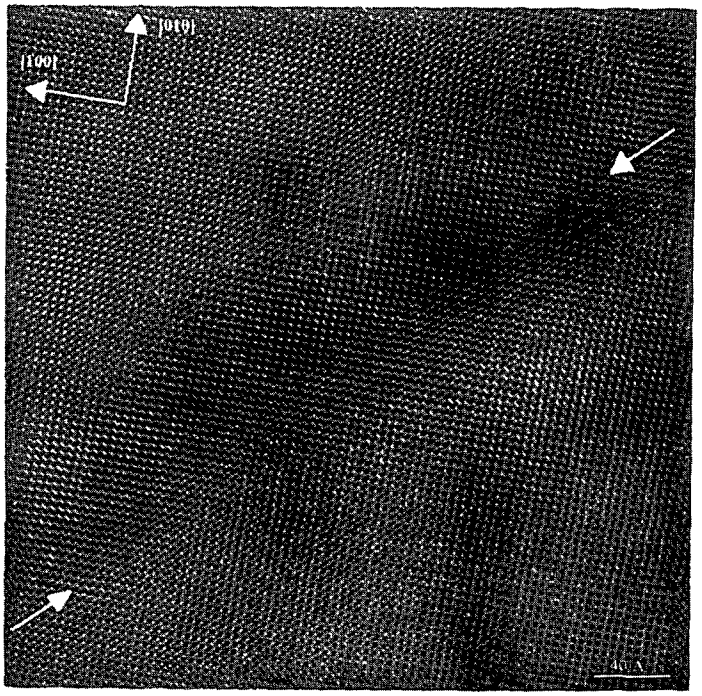


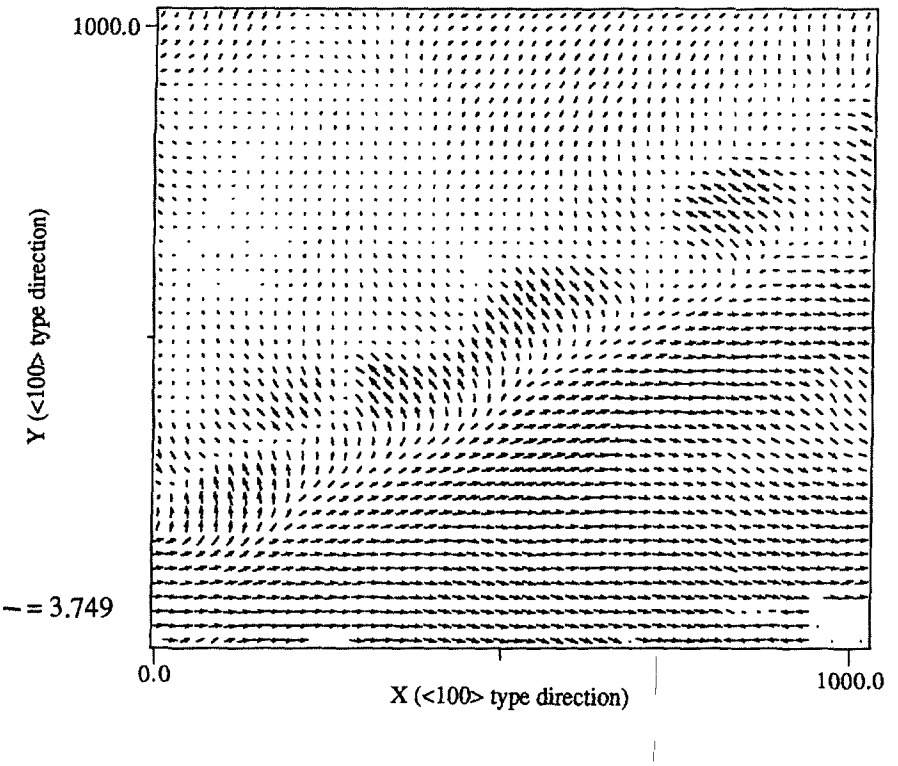


b)

Fig. 20. — *(Continued).*

But certainly the most striking result drawn from these maps is the possibility to access the local configuration of the wall and ultimately features that reveal its interaction with the microstructure. Thus Figure 20a shows how the {110} wall is pinned by the dark defect (arrowed) in the left hand side of the experimental micrograph: the displacements remain roughly regular far away from the defect but clearly spread when the wall gets closer to it. Correspondingly, the wall deviates from its standard {110} plane. In Figure 20b, the wall is less regular and although its general direction remains parallel to {110}, one can observe zig-zag features which could absolutely not be detected in the micrograph. They are easily interpreted in terms of {100} facetting, a configuration which has never been taken into account by theoretical models. Then, energy calculation as well as mobility evaluation must significantly differ from reality: for example, the usually unfavorable "lateral movements" of the domain wall are probably facilitated by this facetting at the expense of the "tip movement" that we have previously observed by the application of an *in situ* electric field in a TEM [6, 27].

*4.4.3. Comparison with the Theoretical Models.* — Relying on a first order "square-rectangle" phase transition prediction [28], we adapted a "soliton" displacement solution to fit the reference ideal tetragonal lattice created from a non-distorted area of our experimental images. The solution is then directly comparable to the displacement vector plots. It is to be noticed that this model takes only into account a pure ferroelastic transition (the order parameter being strain) without considering the polarization. In spite of this approximation, this choice has been preferred since, as we have already indicated, we do not know how to distinguish the effects relative to the variations of the polarization as well as those of atomic displacements.

Furthermore, in order to verify the validity and the accuracy of the quantitative analysis of HRTEM images, we have created an atomic model, corresponding to the above soliton solution, that we have introduced into a contrast simulation software [29]. The HRTEM theoretical images obtained were then treated through the methodology described above: it led to atomic displacement vector plots in total agreement with the direct calculation of the soliton solution (Fig 21). It is then inferred that the technique developed here performs the real local measurement of the 2D-atomic displacements associated with a 90° domain wall.

Finally, comparing Figures 20 and 21, one can immediately observe that the real 90° domain wall structure generally does not correspond to a certain kind of theoretical models: clearly the extension of the lattice perturbations extends farther than what is predicted and irregularities are very frequent. Moreover, the displacement vectors are not as parallel to the walls as could be expected, suggesting that perhaps the distortion of the cells across the walls is not isotropic.

## 5. Summary and Conclusions

The most striking conclusion resulting from this two-pronged work is the perfect convergence for the structural interpretation of what is a 90° domain wall: XRPD brings out structural information about the ferroelectric domain microstructure that is perfectly cross-correlated by the quantitative local HRTEM approach. The 90° domain walls cannot be considered only as twin habit planes, but rather as misfit boundary areas. This new description of domain walls is in agreement with all the observations provided by the studies involving a change in the $BaTiO_3$ ferroelectric microstructure. From our results it is concluded that a "quasi 1D soliton solution" is far too simplistic and does not describe satisfactorily the structure of domain walls in $BaTiO_3$. Attempting to describe the phase transition by a 3D solution remains an exciting challenge.

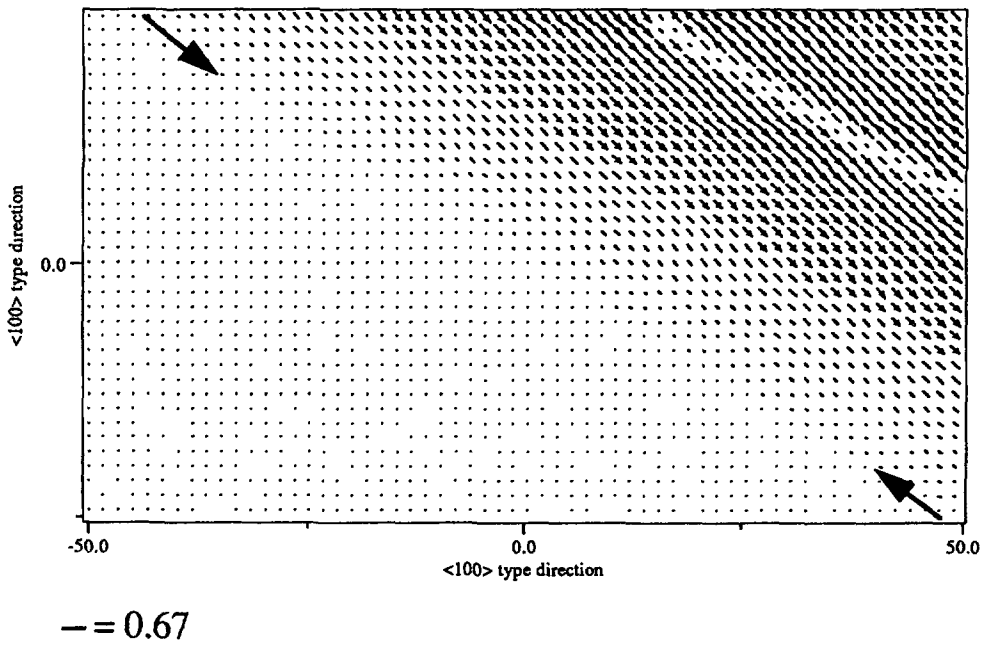


Fig. 21. — Calculated vector plot of a theoretical description of a 90° ferroelastic wall by the "soliton" solution; the origin of the model is located in the lower left corner; the quantitative treatment of a simulated theoretical HRTEM image based on this description gives the same map.

Concerning the XRD approach, the outlook of this work is to propose a theoretical calculation of the $BaTiO_3$ XRD diagram taking into account as much as possible the ferroelectric domain microstructure which has been observed by microscopy and quantitative HRTEM analysis.

The quantitative HRTEM approach presented here can be easily applied to other ferroelectric materials and even to other materials for which HRTEM images can be recorded. Starting from this analysis, some of the present authors are attempting to evaluate the variations of the polarization vector across the walls in order to have access to energy calculations.

## Acknowledgments

Some of the authors (LN, RK, AT) wish to thank sincerely Yvan Montardi and Denis Lavielle (Rhône-Poulenc) for stimulating discussions and for the sintering of the material, and Sandrine Laurent-Fontaine (ENSMP) for her technical assistance. This project has been supported by Rhône-Poulenc, ANVAR, the "École des Mines de Paris", the French "Conférence des Grandes Écoles" and by the Director, Office of Energy Research, Office of the Basic Energy Sciences, Materials Sciences Division of the *U.S. Departement of Energy* under contract No. DE-AC03-76SF00098. The authors are very grateful for the assistance of all the staff and for the use of all the facilities of the National Center for Electron Microscopy.

## References


[1] Merz W.J., Domain formation and domain wall motions in ferroelectric $BaTiO_3$ single crystals, *Phys. Rev.* **95** (1954) 690.

[2] Arlt G., Hennings D. and De With G., Dielectric properties of fine-grained barium titanate ceramic, *J. Appl. Phys.* **58** (1985) 1619.

[3] Michel C., Observations of domains in ferroelectrics and ferromagnetics with a scanning electron microscope, *Philips Tech. Rev.* **36** (1976) 18.

[4] Zhu J.G., Al-Jassim M.M. and Huffman M., Microstructure and domain configurations in ferroelectric $PbTiO_3$ and $Pb(Zr, Ti)O_3$ thin films, *J. Electronic Mat.* **24** (1995) 885.

[5] Yakunin S.I., Shakmanov V.V., Spivak G.V. and Vasil'eva N.V., Microstructure of domains and domain walls in single-crystal films of barium titanate, *Soviet Physics-Solid State* **14** (2) (1972) 310.

[6] Snoeck E., Normand L., Thorel A. and Roucau C., Electron microscopy study of ferroelastic and ferroelectric domain wall motions induced by the *in situ* application of an electric field in $BaTiO_3$, *Phase transitions* **46** (1994) 77.

[7] Saurenbach F. and Terris B.D., Imaging of ferroelectric domain walls by force microscopy, *Appl. Phys. Lett.* **56** (1990) 1703.

[8] Hamazaki S.I., Shimizu F., Kojima S. and Takashige M., AFM observation of 90° domains of $BaTiO_3$ butterfly crystals, *J. Appl. Phys.* **64** (1995) 3660.

[9] Arlt G. and Sasko P., Domain configuration and equilibrium size of domains in $BaTiO_3$ ceramics, *J. Appl. Phys.* **51** (1985) 4956.

[10] Goo E.K.W., Mishra R.K. and Tomas G., Electron microscopy study of the ferroelectric domain wall structure in $Pb(Zr_{0\,52}Ti_{0\,48})O_3$, *J. Appl. Phys.* **52** (1981) 2940.

[11] Ju Chen and Duan Feng, HREM study of {110}p ferroelectric domain walls in $KNbO_3$, Pro. XIth Int. Cong. on Electron Microscopy, Kyoto (1986) p. 1321.

[12] Dennis M.D. and Bradt R.C., Thickness of 90° ferroelectric domain walls in (Ba, Pb)$TiO_3$ single crystal, *J. Appl. Phys.* **45** (1974) 1931.

[13] Zhu Y., Suenaga M. and Xu Y., TEM studies on twin boundariy in $YBa_2Cu_3O_{7-\delta}$ and $YBa_2(Cu_{0\,98}M_{0\,02})_3O_7$ (M = Zn, Al), *J. Mater. Rev.* **5** (1990) 1380.

[14] Zhu Y. and Suenaga M., Twinning dislocations in $YBa_2Cu_3O_{7-\delta}$ superconductors, *Philos. Mag. A* **66** (1992) 457.

[15] Bursill L.A. and Lin P.J., Electron microscopic studies of ferroelectric crystals, *Ferroelectrics* **70** (1986) 191.

[16] Tsai F., Khiznishenko V. and Cowley J.M., High resolution electron microscopy of 90° ferroelectric domain boundaries in $BaTiO_3$ and $Pb(Zr_{0\,52}Ti_{0\,48})O_3$, *Ultramicroscopy* **45** (1992) 5.

[17] Normand L., Thorel A. and Montardi Y., HREM study of ferooelectric domain walls in Barium titanate, Microscopy Society of America 52nd meeting, G.W. Bailey & A.J. Garratt-Reed, Eds., New Orleans (1994) 566.

[18] Zhang X., Hashimoto T. and Joy D.C., Electron holography study of ferroelectric domain walls, *Appl. Phys. Lett.* **60** (1992) 784.

[19] Stemmer S., Streiffer S.K., Ernst F. and Rühle M., Atomistic structure of 90° domain walls in ferroelectric $PbTiO_3$ thin films, *Philos. Mag. A* **71** (1995) 713.

[20] Cao Wenwu and Cross L.E., Theory of ferroelectric twin structure in ferrolelectric perovskites with a first-order phase transition, *Phys. Rev. B* **44** (1991) 5.

[21] Valot C.M., Berar J.F., Courtois C., Maglione M., Mesnier M. and Nièpce J C., X-ray diffraction diagram evolution of a $BaTiO_3$ ceramic under an electric field, *Ferroelectrics Letters* **17** (1994) 5.

[22] Williamson G.K. and Hall W.H., X-ray line broadening from filed aluminium and wolfram, *Acta. Met.* **1** (1953) 22.

[23] Valot C.M., Floquet N., Perriat P., Mesnier M. and Nièpce J.C., Ferroelectric domains in $BaTiO_3$ powders and ceramics evidenced by X-ray diffraction, *Ferroelectrics* **172** (1995) 235.

[24] Sarrazin P., Thierry B. and Nièpce J.C., Forming pressure dependence of the ferroelectric domain structure in green barium titanate pellets, *J. Europ Ceram. Soc.* **15** (1995) 623.

[25] Valot C.M., Floquet N., Mesnier M. and Nièpce J.C., A new possibility for powder diffraction: the characterization of the domain microstructure in a ferroelectric material, EPDIC IV Chester (1995).

[26] Normand L., Kilaas R. Montardi Y. and Thorel A , Study of the structure of ferroelectric domain walls in barium titanate ceramics, *Materials Science Forum* **207-209** (1996) 317.

[27] Snoeck E., Roucau C., Baules P., Casanove M.J., Fagot M., Astie B. and Degauque J., Use of *in situ* TEM experiments for phase transition studies, *Microscopie, Microanalyse, Microstructure* **4** (1993) 249.

[28] Jacobs A.E., Solitons of the square-rectangular martensitic transformation, *Phys. Rev. B* **31** (1985) 5984.

[29] MacTempas ©, RKCS, by Roar Kilaas (1988).